STRUCTURAL BIOLOGY COMMUNICATIONS

ISSN 2053-230X

Crystal structure of the catalytic domain of human RPTPH

Myeongbin Kim and Seong Eon Ryu*

Department of Bioengineering, College of Engineering, Hanyang University, Seoul 04673, Republic of Korea.
*Correspondence e-mail: ryuse@hanyang.ac.kr

Received 1 April 2022
Accepted 10 June 2022

Edited by K. K. Kim, Sungkyunkwan University School of Medicine, Republic of Korea

Keywords: human RPTPH; crystal structure; specific inhibitor development; loop conformation; colorectal cancer; hepatic carcinoma.

PDB reference: human RPTPH, 7xc0

Supporting information: this article has supporting information at journals.iucr.org/f

Receptor-type protein tyrosine phosphatases (RPTPs) receive extracellular stimuli and transfer them into cells. They regulate cell growth, differentiation and death via specific signals. They have also been implicated in cancer, diabetes and neurological diseases. RPTPH, a member of the type 3 RPTP (R3-PTP) family, is an important regulator of colorectal cancer and hepatic carcinoma. Despite its importance in drug development, the structure of RPTPH has not yet been resolved. Here, the crystal structure of the catalytic domain of RPTPH was determined at 1.56 Å resolution. Despite similarities to other R3-PTPs in its overall structure, RPTPH exhibited differences in its loop regions and side-chain conformations. Compared with other R3-PTPs, RPTPH has unique side chains near its active site that may confer specificity for inhibitor binding. Therefore, detailed information on the structure of RPTPH provides clues for the development of specific inhibitors.

1. Introduction

Protein tyrosine phosphatases (PTPs) comprise more than a hundred genes in the human genome that control phosphorylation levels in cells (Tonks, 2006). They regulate cellular signalling pathways associated with cell survival, apoptosis and proliferation. Hence, their malfunction has been reported to cause cancer, diabetes and neurological disorders (Zhang *et al.*, 2019; Wiesmann *et al.*, 2004; Jeffrey *et al.*, 2007). Receptor-type PTPs (RPTPs), a subfamily of PTP proteins, are membrane proteins with a single transmembrane motif together with an extracellular signal-receiver region and an intracellular PTP catalytic region (den Hertog *et al.*, 1999; Mohebiany *et al.*, 2013). The catalytic domain, similar to those of other PTPs, has a signature motif (HCX_5R) in the P-loop and a conserved aspartic acid in the WPD (Trp–Pro–Asp motif) loop.

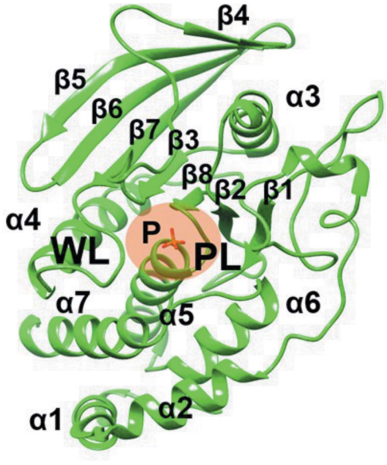

The RPTP subfamily consists of 21 proteins that are categorized into eight types (R1/R6, R2a, R2b, R3, R4, R5, R7 and R8) depending on the composition of their intracellular and extracellular domains (Alonso & Pulido, 2016). Type 3 RPTPs (R3-PTPs) have a transmembrane motif, tandem extracellular fibronectin type III (FN3) domains and a single intracellular phosphatase domain. The extracellular FN3 domains regulate the phosphatase activity by interacting with ligand molecules or other proteins, whereas the intracellular phosphatase domain removes phosphate groups from substrates.

Five RPTP proteins, RPTPB (VE-PTP), RPTPJ (DEP-1/CD148), RPTPO (GLEPP1), RPTPQ and RPTPH, are grouped together as the R3-PTP type of RPTPs (Alonso & Pulido, 2016). Among these, RPTPH, also known as stomach

cancer-associated protein-tyrosine phosphatase-1, is involved in the AKT signaling pathway and regulates cell apoptosis and T-cell function (Ito *et al.*, 2003; Takada *et al.*, 2002). RPTPH has been implicated in various disorders, such as colorectal cancer and hepatic carcinoma (Sato *et al.*, 2015; Seo *et al.*, 1997). While the structures of other R3-PTPs have been determined (Evdokimov *et al.*, 2006; Barr *et al.*, 2009; Almo *et al.*, 2007; Yu *et al.*, 2013), that of RPTPH remains unresolved. Here, we report the crystal structure of the catalytic domain of RPTPH at 1.56 Å resolution. Comparison of the structure of RPTPH with those of other R3-PTPs revealed structural differences in the active-site residues and loop conformations despite the similarity in their overall structures (sequence similarities of 55–60%), indicating the unique role of each R3-PTP enzyme in substrate recognition and regulatory protein interaction. These unique features may be exploited for the development of specific inhibitors as therapeutic agents against diseases associated with R3-PTPs.

2. Materials and methods

2.1. Macromolecule production and crystallization

To overexpress the protein for crystallization, we prepared a plasmid encoding the catalytic domain of human RPTPH (residues 798–1086; UniProt Q9HD43-1) by subcloning the amplified insert gene into the pET-28a vector using NdeI and XhoI restriction enzymes. Two mutations, C818A and C1020S, were introduced to prevent oxidation of the protein. Detailed information on protein expression, purification and crystallization has previously been reported (Kim & Ryu, 2021). Briefly, *Escherichia coli* BL21(DE3) cells transformed with the pET-28a vector encoding the mutated RPTPH were cultured in Luria–Bertani medium and protein overexpression was induced with isopropyl β-D-1-thiogalactopyranoside. The harvested cells were lysed and the protein was purified by nickel affinity chromatography. The purified protein was pooled, concentrated to 20 mg ml^{-1} and stored at −70°C. The crystal used for data collection was obtained from a drop consisting of a 2:1 ratio of protein and reservoir [0.1 *M* MES–NaOH pH 6.5, 13%(*v*/*v*) PEG MME 550] solutions.

2.2. Structure solution and refinement

Data were collected from the RPTPH crystal on beamline 7A at the Pohang Accelerator Laboratory. The crystal was flash-cooled in a nitrogen stream at 100 K after soaking in a cryoprotectant solution [0.1 *M* MES–NaOH pH 6.5, 40%(*v*/*v*) PEG MME 550, 10% glycerol] for 30 s. *HKL*-2000 (Otwinowski *et al.*, 2003) was used to process, integrate and scale the data. The merged data were used in molecular replacement (MR) using the *Phenix* suite (Liebschner *et al.*, 2019). For MR, the crystal structure of the catalytic domain of the R3-PTP RPTPJ (PDB entry 2nz6; Barr *et al.*, 2009), with 47.9% sequence identity to the catalytic domain of RPTPH, was used as an initial search model.

The target protein for the MR search was prepared from the RPTPJ structure (PDB entry 2nz6) using *Sculptor* (Bunkóczi & Read, 2011). An MR search using *Phaser* (McCoy *et al.*, 2007) found a solution with scores of TFZ = 30.9 and LLG = 914.5; MR calculations showed a single macromolecule in the asymmetric unit. The structure was refined using *phenix.refine* (Liebschner *et al.*, 2019), with manual modifications implemented using *Coot* (Emsley *et al.*, 2010). The final structure had R_{work} and R_{free} values of 17.8% and 20.7%, respectively, at 1.56 Å resolution. Table 1 presents the data-collection and refinement statistics.

Table 1
Structure solution and refinement.

Values in parentheses are for the outer shell.

PDB entry	7xc0
Space group	$P3_2$
Resolution range (Å)	24.45–1.56 (1.62–1.56)
a, *b*, *c* (Å)	56.46, 56.46, 80.45
α, β, γ (°)	90.00, 90.00, 120.00
Total No. of reflections	149225
No. of unique reflections	38539
R_{merge}	0.069 (0.32)
$\langle I/\sigma(I)\rangle$	10.6 (2.9)
$CC_{1/2}$	0.997 (0.389)
Multiplicity	3.9
Completeness (%)	94.2 (87.7)
No. of reflections, working set	38471 (3574)
No. of reflections, test set	1980 (174)
R_{work}/R_{free} (%)	17.81/20.74
No. of non-H atoms	
Protein	2318
Ligand	5
Water	189
Protein residues	287
Average *B* factors (Å^2)	
Protein	31.0
Ligand	22.1
Water	39.8
R.m.s. deviations	
Bond lengths (Å)	0.003
Angles (°)	0.6
Ramachandran plot† (residues)	
Favored	276
Allowed	8
Outliers	1

† The Ramachandran plot was calculated by *MolProbity*, which excluded the N- and C-terminal residues during calculation.

3. Results and discussion

The structure of the catalytic domain of RPTPH consists of a typical PTP-fold composed of β-strands surrounded by α-helices. Eight β-strands ($\beta1\downarrow\beta2\uparrow\beta8\uparrow\beta3\uparrow\beta7\uparrow\beta6\downarrow\beta5\uparrow\beta4\downarrow$) are placed in the central region, flanked by six α-helices ($\alpha1$, $\alpha2$, $\alpha4$, $\alpha5$, $\alpha6$ and $\alpha7$) on one side and an additional α-helix ($\alpha3$) on the other side (Fig. 1*a*). The WPD loop is placed between $\beta7$ and $\alpha4$, showing a 'closed' conformation. Consequently, Asp986, the general acid in the catalytic reaction, is close to the active-site pocket (Figs. 1*a* and 1*b*).

A phosphate ion was observed in the active-site pocket, which was stabilized by an ionic interaction with Arg1026 and by hydrogen bonds to the P-loop backbone amides (Figs. 1*c* and 1*d*). The active site of PTPs is known to dephosphorylate the substrates using the conserved cysteine and arginine residues in the P-loop, which hold a phosphate group in this

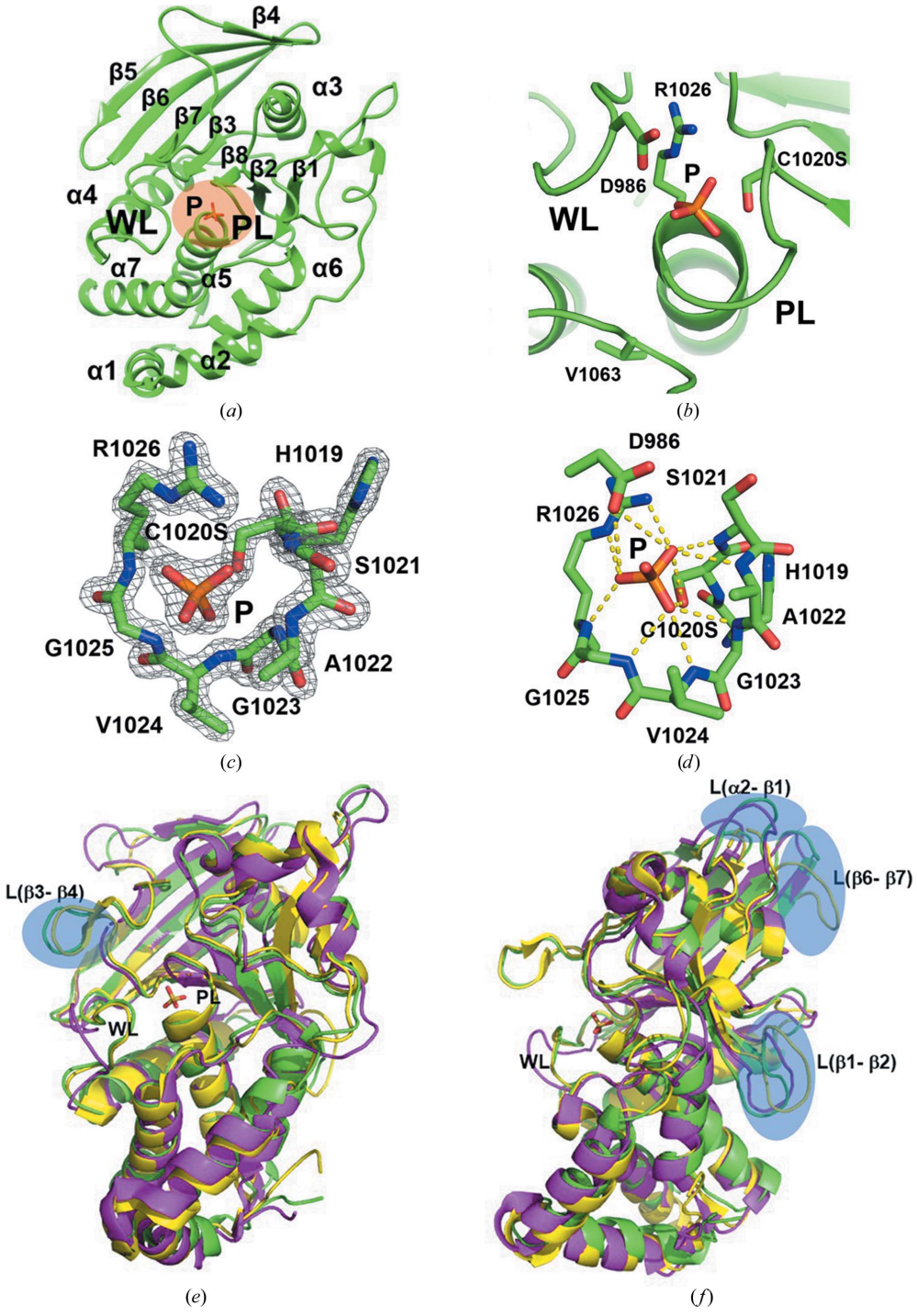

Figure 1
Structure of RPTPH. (*a*) Ribbon diagram of the structure of RPTPH shown with labels for the secondary-structural elements as determined using the secondary-structure determination algorithm of *PyMOL* (*β*1, Ala877–Met880; *β*2, Glu888–Thr892; *β*3, Thr914–Met917; *β*4, Cys940–His942; *β*5, Leu945–Val954; *β*6, Trp958–Gln967; *β*7, Gln971–Tyr981; *β*8, Ile1017–His1019; *α*1, Ala802–Glu813; *α*2, Ala818–Leu829; *α*3, Val900–Gln910; *α*4, Pro993–Gln1009; *α*5, Gly1025–Glu1043; *α*6, Pro1048–Ser1058; *α*7, Glu1066–Gln1082). The WPD and P-loops are labeled WL and PL, respectively. The active site is marked as an orange circle. The active site-bound phosphate (labeled P) is represented as a stick model. (*b*) Conformation of the active-site residues. Representative residues (Asp986, Arg1026 and Val1063) in the active-site region are presented as stick models. The catalytic cysteine (labeled C1020S to indicate the cysteine-to-serine mutation of this residue) is also presented. The phosphate ion is labeled P and the WPD and P-loops are labeled WL and PL, respectively. (*c*) The $2F_o - F_c$ electron-density map (contoured at 2.0σ) of the P-loop residues and the phosphate ion in the active site of RPTPH. The catalytic cysteine is labeled C1020S to indicate the cysteine-to-serine mutation of this residue. (*d*) Interactions between the phosphate ion and active-site amino acids are presented as yellow dashed lines. The presented interactions have interaction distances of 2.7–3.4 Å. The catalytic cysteine is labeled C1020S to indicate the cysteine-to-serine mutation of this residue. (*e*, *f*) Structural superposition of R3-PTPs with RPTPH. The ribbon diagram of RPTPH (green) was superposed with those of other R3-PTPs, namely RPTPB (PDB entry 2i4g, yellow; Evdokimov *et al.*, 2006) and RPTPQ (PDB entry 4ikc, magenta; Yu *et al.*, 2013). The WPD and P-loops are labeled WL and PL, respectively. The view in (*f*) is a rotation of approximately 90° around the vertical axis from that in (*e*).

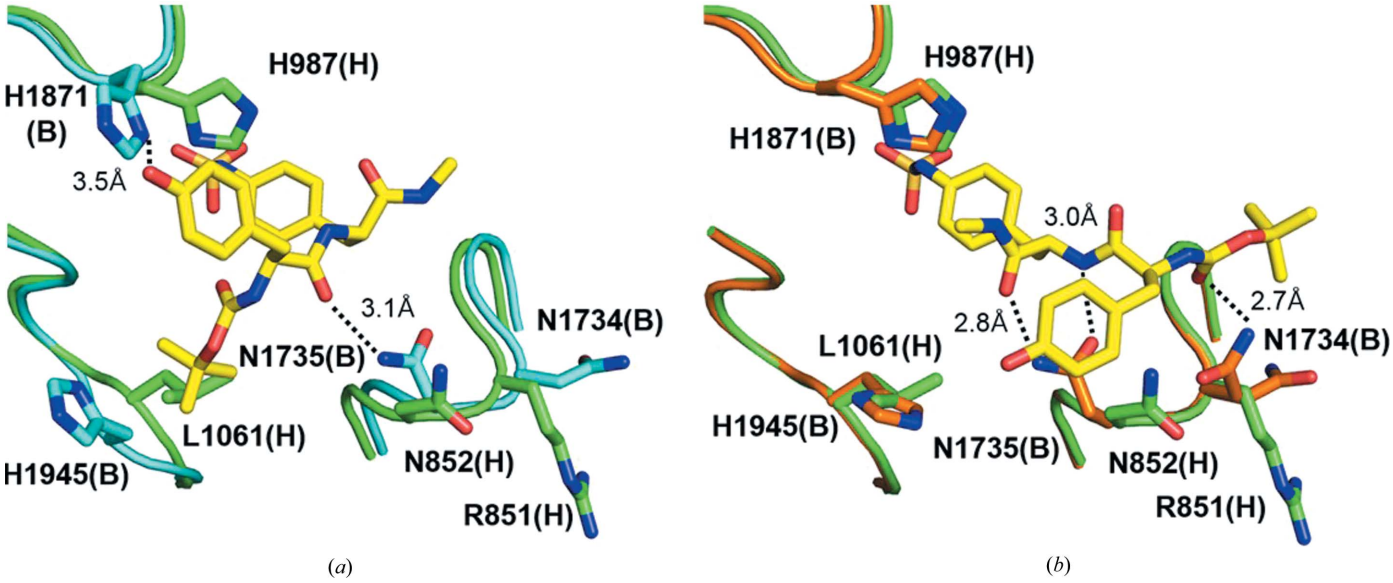

Figure 2
Differences in the inhibitor-binding sites. The inhibitor-binding region of RPTPB [cyan in (*a*) and orange in (*b*)] and bound inhibitor (yellow) (PDB entries 2i4g and 2i4h, respectively) were compared with the corresponding region of RPTPH (green). Two types of inhibitor-binding modes, (*a*) and (*b*), were reported for RPTPB (Evdokimov *et al.*, 2006; see text for details). Representative interactions between RPTPB and its inhibitors are displayed as dashed lines. The interaction distances are noted on the dashed lines. RPTPH does not make the interactions found in RPTPB, indicating a different inhibitor-binding specificity. Residues of RPTPH and RPTPB are labeled with (H) or (B), respectively, at the end of their names.

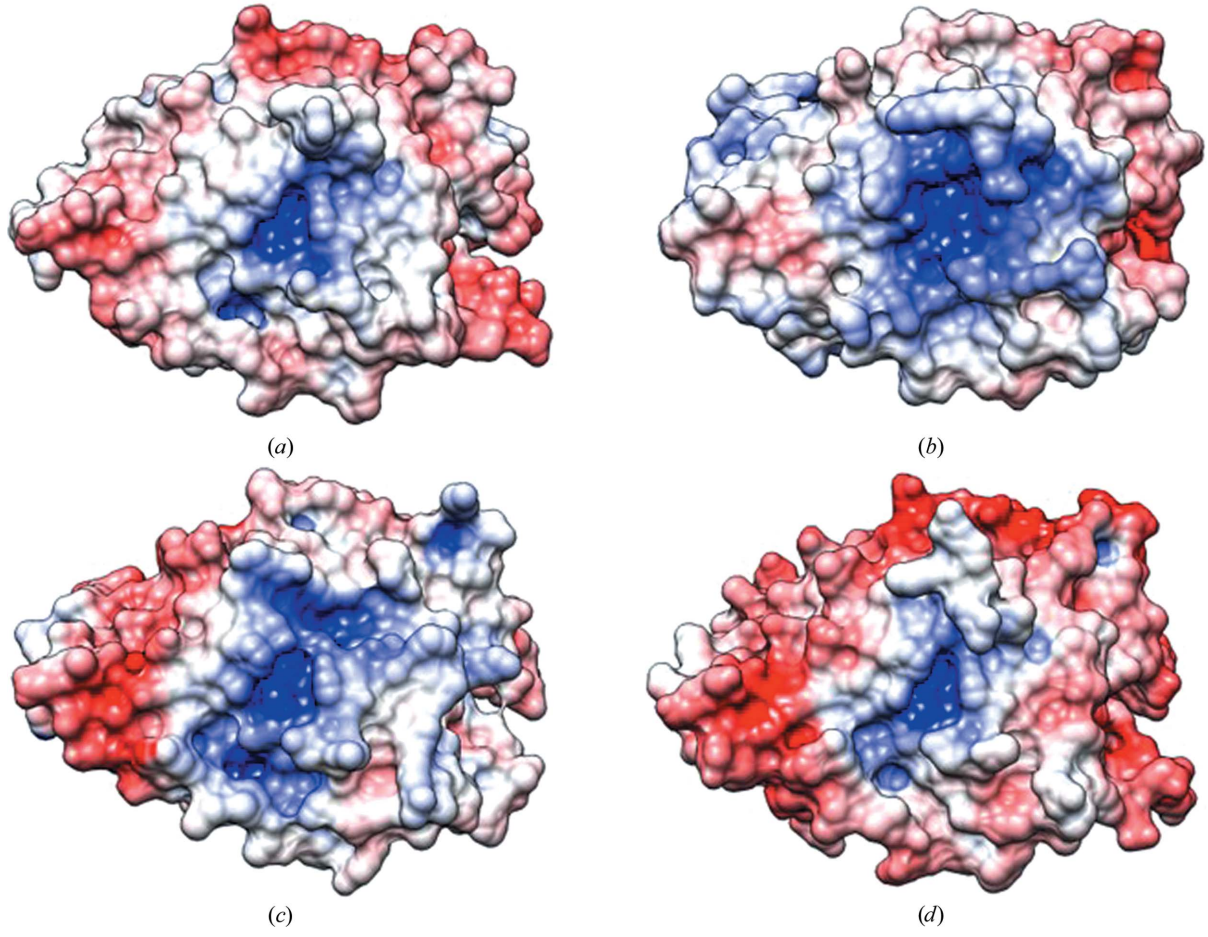

Figure 3
Electrostatic surfaces of R3-PTPs. Electrostatic surfaces of R3-PTPs are presented in the same orientation (red, negative charge potential; blue, positive charge potential). The central region of each representation corresponds to the active-site pocket. (*a*) RPTPH, (*b*) RPTPB (PDB entry 2i4g; Evdokimov *et al.*, 2006), (*c*) RPTPJ (PDB entry 2nz6; Barr *et al.*, 2009) and (*d*) RPTPO (PDB entry 2g59; Almo *et al.*, 2007).

pocket (Fig. 1*b*). A Ramachandran outlier (Val1063) was detected using *MolProbity* (Chen *et al.*, 2010). The electron density for Val1063 was well resolved and the residue was found to play an important role in the formation of a hydrophobic core near the P-loop (Fig. 1*b*). The Val1063-containing loop shows close interactions with the P-loop, contributing to stabilization of the P-loop conformation.

The overall structure of RPTPH is similar to those of other R3-PTPs (average C^{α} r.m.s.d. values of 1.4, 1.4, 1.7 and 2.1 Å with RPTPB, RPTPO, RPTPJ and RPTPQ, respectively); however, differences were observed in the loop regions (Figs. 1*e* and 1*f*). The conformation of the $\beta3$–$\beta4$ loop in RPTPH resembled that in RPTPB but differed from that in RPTPQ (Fig. 1*e*). This M6 loop aids in the recognition of phosphatidylinositide substrates in RPTPQ (Yu *et al.*, 2013). In comparison, RPTPH dephophorylates protein substrates (Ito *et al.*, 2003), consistent with the difference in conformation of the loop. Other loops exhibiting pronounced differences among R-PTPs include the $\alpha1$–$\beta1$, $\beta6$–$\beta7$ and $\beta1$–$\beta2$ loops, which are located on the surface opposite the active site (Fig. 1*f*). The flexible $\alpha2$–$\beta1$ loop was not observed in the structure of RPTPB (Fig. 1*f*), while the $\beta6$–$\beta7$ and $\beta1$–$\beta2$ loops exhibited large deviations from those in RPTPH and RPTPQ (Fig. 1*f*). The diverse conformations of these loops among the different R3-PTPs indicate that the surface opposite the active site may act as a site for specific interactions with regulatory proteins.

The structure of the catalytic domain of RPTPB in complex with inhibitors revealed the specific interactions between the protein and its inhibitors (Evdokimov *et al.*, 2006). The inhibitor *N*-(*t*-butoxycarbonyl)-L-tyrosyl-*N*-methyl-4-(sulfoamino)-L-phenylalanylamide interacts with RPTPB in two different modes (Evdokimov *et al.*, 2006). Superposition of the RPTPH structure with those of RPTPB–inhibitor complexes revealed that the inhibitor-interacting residues were not conserved, indicating that development of specific inhibitors would be possible by exploiting the differences in the side chains near the active-site pocket (Fig. 2). In the first inhibitor-binding mode (Fig. 2*a*) the inhibitor interacted with the side chains of His1871(B) and His1945(B). In the structure of RPTPH, the conformations of the two residues are changed: His987(H) has a different conformation, while Leu1061(H) has a different side chain and conformation. In the second mode (Fig. 2*b*) the inhibitor interacts with the side chains of Asn1734(B) and Asn1735(B); the two residues of RPTPH corresponding to these residues have a different side chain [Arg851(H)] or conformation [Asn852(H)]. The van der Waals surface and charge representations of members of the R3-PTPs show differences in the active-site pocket (Fig. 3), indicating that specific inhibitor interactions can be exploited to design selective inhibitors for different R3-PTP members.

Acknowledgements

We thank the staff members of beamline 7A at the Pohang Accelerator Laboratory (PAL) for diffraction data collection.

Funding information

This work was supported by biomedical technology development projects of National Research Foundation, Korea (NRF-2015M3A9B5030302 and NRF-2021M3A9G8024747).

References

Almo, S. C., Bonanno, J. B., Sauder, J. M., Emtage, S., Dilorenzo, T. P., Malashkevich, V., Wasserman, S. R., Swaminathan, S., Eswaramoorthy, S., Agarwal, R., Kumaran, D., Madegowda, M., Ragumani, S., Patskovsky, Y., Alvarado, J., Ramagopal, U. A., Faber-Barata, J., Chance, M. R., Sali, A., Fiser, A., Zhang, Z. Y., Lawrence, D. S. & Burley, S. K. (2007). *J. Struct. Funct. Genomics*, **8**, 121–140.

Alonso, A. & Pulido, R. (2016). *FEBS J.* **283**, 1404–1429.

Barr, A. J., Ugochukwu, E., Lee, W. H., King, O. N., Filippakopoulos, P., Alfano, I., Savitsky, P., Burgess-Brown, N. A., Müller, S. & Knapp, S. (2009). *Cell*, **136**, 352–363.

Bunkóczi, G. & Read, R. J. (2011). *Acta Cryst.* D**67**, 303–312.

Chen, V. B., Arendall, W. B., Headd, J. J., Keedy, D. A., Immormino, R. M., Kapral, G. J., Murray, L. W., Richardson, J. S. & Richardson, D. C. (2010). *Acta Cryst.* D**66**, 12–21.

den Hertog, J., Blanchetot, C., Buist, A., Overvoorde, J., van der Sar, A. & Tertoolen, L. G. (1999). *Int. J. Dev. Biol.* **43**, 723–733.

Emsley, P., Lohkamp, B., Scott, W. G. & Cowtan, K. (2010). *Acta Cryst.* D**66**, 486–501.

Evdokimov, A. G., Pokross, M., Walter, R., Mekel, M., Cox, B., Li, C., Bechard, R., Genbauffe, F., Andrews, R., Diven, C., Howard, B., Rastogi, V., Gray, J., Maier, M. & Peters, K. G. (2006). *Acta Cryst.* D**62**, 1435–1445.

Ito, T., Okazawa, H., Maruyama, K., Tomizawa, K., Motegi, S., Ohnishi, H., Kuwano, H., Kosugi, A. & Matozaki, T. (2003). *J. Biol. Chem.* **278**, 34854–34863.

Jeffrey, K. L., Camps, M., Rommel, C. & Mackay, C. R. (2007). *Nat. Rev. Drug Discov.* **6**, 391–403.

Kim, M. & Ryu, S. E. (2021). *Biodesign*, **9**, 55–58.

Liebschner, D., Afonine, P. V., Baker, M. L., Bunkóczi, G., Chen, V. B., Croll, T. I., Hintze, B., Hung, L.-W., Jain, S., McCoy, A. J., Moriarty, N. W., Oeffner, R. D., Poon, B. K., Prisant, M. G., Read, R. J., Richardson, J. S., Richardson, D. C., Sammito, M. D., Sobolev, O. V., Stockwell, D. H., Terwilliger, T. C., Urzhumtsev, A. G., Videau, L. L., Williams, C. J. & Adams, P. D. (2019). *Acta Cryst.* D**75**, 861–877.

McCoy, A. J., Grosse-Kunstleve, R. W., Adams, P. D., Winn, M. D., Storoni, L. C. & Read, R. J. (2007). *J. Appl. Cryst.* **40**, 658–674.

Mohebiany, A. N., Nikolaienko, R. M., Bouyain, S. & Harroch, S. (2013). *FEBS J.* **280**, 388–400.

Otwinowski, Z., Borek, D., Majewski, W. & Minor, W. (2003). *Acta Cryst.* A**59**, 228–234.

Sato, T., Soejima, K., Arai, E., Hamamoto, J., Yasuda, H., Arai, D., Ishioka, K., Ohgino, K., Naoki, K., Kohno, T., Tsuta, K., Watanabe, S., Kanai, Y. & Betsuyaku, T. (2015). *Oncol. Rep.* **34**, 1137–1145.

Seo, Y., Matozaki, T., Tsuda, M., Hayashi, Y., Itoh, H. & Kasuga, M. (1997). *Biochem. Biophys. Res. Commun.* **231**, 705–711.

Takada, T., Noguchi, T., Inagaki, K., Hosooka, T., Fukunaga, K., Yamao, T., Ogawa, W., Matozaki, T. & Kasuga, M. (2002). *J. Biol. Chem.* **277**, 34359–34366.

Tonks, N. K. (2006). *Nat. Rev. Mol. Cell Biol.* **7**, 833–846.

Wiesmann, C., Barr, K. J., Kung, J., Zhu, J., Erlanson, D. A., Shen, W., Fahr, B. J., Zhong, M., Taylor, L., Randal, M., McDowell, R. S. & Hansen, S. K. (2004). *Nat. Struct. Mol. Biol.* **11**, 730–737.

Yu, K. R., Kim, Y. J., Jung, S.-K., Ku, B., Park, H., Cho, S. Y., Jung, H., Chung, S. J., Bae, K. H., Lee, S. C., Kim, B. Y., Erikson, R. L., Ryu, S. E. & Kim, S. J. (2013). *Acta Cryst.* D**69**, 1522–1529.

Zhang, Y., Roos, M., Himburg, H., Termini, C. M., Quarmyne, M., Li, M., Zhao, L., Kan, J., Fang, T., Yan, X., Pohl, K., Diers, E., Gim, H. J., Damoiseaux, R., Whitelegge, J., McBride, W., Jung, M. E. & Chute, J. P. (2019). *Nat. Commun.* **10**, 3667.